ELSEVIER

Journal of Chromatography A, 852 (1999) 3–23

JOURNAL OF CHROMATOGRAPHY A

Network modeling of the convective flow and diffusion of molecules adsorbing in monoliths and in porous particles packed in a chromatographic column

J.J. Meyers, A.I. Liapis*

Department of Chemical Engineering and Biochemical Processing Institute, University of Missouri-Rolla, Rolla, MO 65409-1230, USA

Abstract

A cubic lattice network of interconnected pores was constructed to represent the porous structure existing in a monolith (continuous bed) or in a column packed with porous chromatographic particles. Expressions were also constructed and utilized to simulate, through the use of the pore network model, the intraparticle interstitial velocity and pore diffusivity of adsorbate molecules in porous chromatographic particles or in monoliths under retained and unretained conditions. The combined effects of steric hindrance at the entrance to the pores and frictional resistance within the pores, as well as the effects of pore size, pore connectivity, n_T, of the porous network, molecular size of adsorbate and ligand (active site), and the fractional saturation of adsorption sites (ligands), have been considered. The results for the adsorption systems studied in this work, indicate that the obstruction effects on the intraparticle interstitial velocity, due to (a) the thickness of the immobilized layer of active sites and (b) the thickness of the adsorbed layer, are small and appear to be insignificant when they are compared with the very significant effect that the value of the pore connectivity, n_T, has on the magnitude of the intraparticle interstitial velocity. The effective pore diffusion coefficient of the adsorbate molecules was found to decline with increasing molecular size of ligand, with increasing fractional saturation of the active sites or with diminishing pore size, and with decreasing pore connectivity, n_T. The results also show that the magnitude of the interstitial fluid velocity is many times larger than the diffusion velocity of the adsorbate molecules within the porous adsorbent particles. Furthermore, the results clearly show that the intraparticle interstitial velocity and the pore diffusivity of the adsorbate increase significantly as the value of the pore connectivity, n_T, of the porous medium increases. The results of this work indicate that the pore network model and the expressions presented in this work, could allow one, for a given porous adsorbent, adsorbate, ligand (active site), and interstitial column fluid velocity, to determine in an a priori manner the values of the intraparticle interstitial velocity and pore diffusivity within the monolith or within the porous adsorbent particles as the fractional saturation of the active sites changes. The values of these transport parameters could then be employed in the macroscopic models that could predict the dynamic behavior, scale-up, and design of chromatographic systems. The theoretical results could also have important implications in the selection of a ligand as well as in the selection and construction of an affinity porous matrix.

Keywords: Diffusion; Porous particles; Intraparticle convective flow; Adsorbents; Pore size distribution; Pore connectivity; Monolith stationary phases; Stationary phases, LC; Pore network model; Mathematical modeling

*Corresponding author.

0021-9673/99/$ – see front matter
PII: S0021-9673(99)00443-4

1. Introduction

Affinity adsorption systems with high separation speeds could be obtained (i) in columns packed with chromatographic porous particles whose porous structure allows the transport of the molecules of interest to occur by intraparticle convective fluid flow and pore diffusion [1–22], and (ii) in monoliths (continuous beds) having both large pores allowing convective fluid flow and smaller pores for diffusion [22–29]. Meyers and Liapis [22] constructed a pore network model (cubic lattice network) to represent the porous structure in a column packed with porous chromatographic particles and developed expressions that were used to determine, through the utilization of the pore network model, the values of the intraparticle interstitial fluid velocity, $v_{p,i}$, and pore diffusivity, D_p, of a solute in an a priori manner under unretained conditions and when the molecular volume, $\bar{V}_B$, of the immobilized active sites is negligible ($V_B \cong 0$). It should be noted that the pore network model constructed by Meyers and Liapis [22] could also be used to determine, in an a priori manner, the values of the convective velocity and pore diffusivity of a solute in monoliths.

In this work, expressions are constructed and are employed in the pore network modeling approach developed by Meyers and Liapis [22] in order to determine in an a priori manner the intraparticle velocity and pore diffusion coefficient of adsorbate molecules in monoliths and in chromatographic columns packed with porous particles and operated under retained or unretained conditions. The molecular volume of the immobilized active sites could be greater than or equal to zero ($V_B \geqslant 0$).

2. Model formulation

The chromatographic column packed with porous adsorbent particles or the monolith (continuous bed) is topologically mapped onto a cubic lattice network of interconnected cylindrical pores and the lattice employed in our work has a regular array of nodes (the lattice size L is the same along the x, y, and z space coordinates of the network, and thus, $x \times y \times z$: $L \times L \times L$) that are connected to each other by bonds (pores) of the network. The pore connectivity, n_T, is defined as the number of bonds (pores) connected to a single node of the lattice. In this work, the nodes of the cubic lattice are considered to have no volume in the network while the bonds (pores) of the network are considered to provide the pore volume of the network (bond percolation). For mediums whose structure is made from fibers, it could be possible to consider that all the volume of the network is contained in the nodes (sites) and the bonds of the network have no volume (site percolation). In Fig. 1, a schematic representation of a column section packed with porous particles is shown, and the composite pore size distribution representing the porous structure of a small finite section of the column packed with porous particles having macropores and micropores (the pore size distribution of the pores of the particles is considered to be bimodal) is constructed topologically in the lattice by randomly assigning cylindrical pores to the bonds in the cubic network. It should be noted that the schematic representation of the model porous medium in Fig. 1 reflects an ''actual'' model porous medium structure taking into account pore length and pore connectivity variability. For the realistic representation of the porous structure in the column, the pore size distribution of the network (model porous medium) should be similar to the pore size distributions encountered in the interstitial pores and in the pores of the particles. In a column being in operation in practice, the interstitial and intraparticle pores are correlated [30], and thus, cannot be assigned to the network randomly. Therefore, in order to generate a realistic model porous medium (network) representation of the packed column, the interstitial pores are assigned [22,31,32] in a semi-random manner to a percolating cluster which transects the lattice. The assignment of the intraparticle pores in the network is completely random. It should be noted here that there could exist certain porous chromatographic particles in which the macropores are not randomly distributed relative to the micropores (non-random bidisperse pore network); in such a case, our approach in constructing the intraparticle pore network is slightly modified by employing in the assignment of the intraparticle pores the procedure reported in ref. [22]. In the case of a monolith (continuous bed), the interstitial pores in Fig. 1

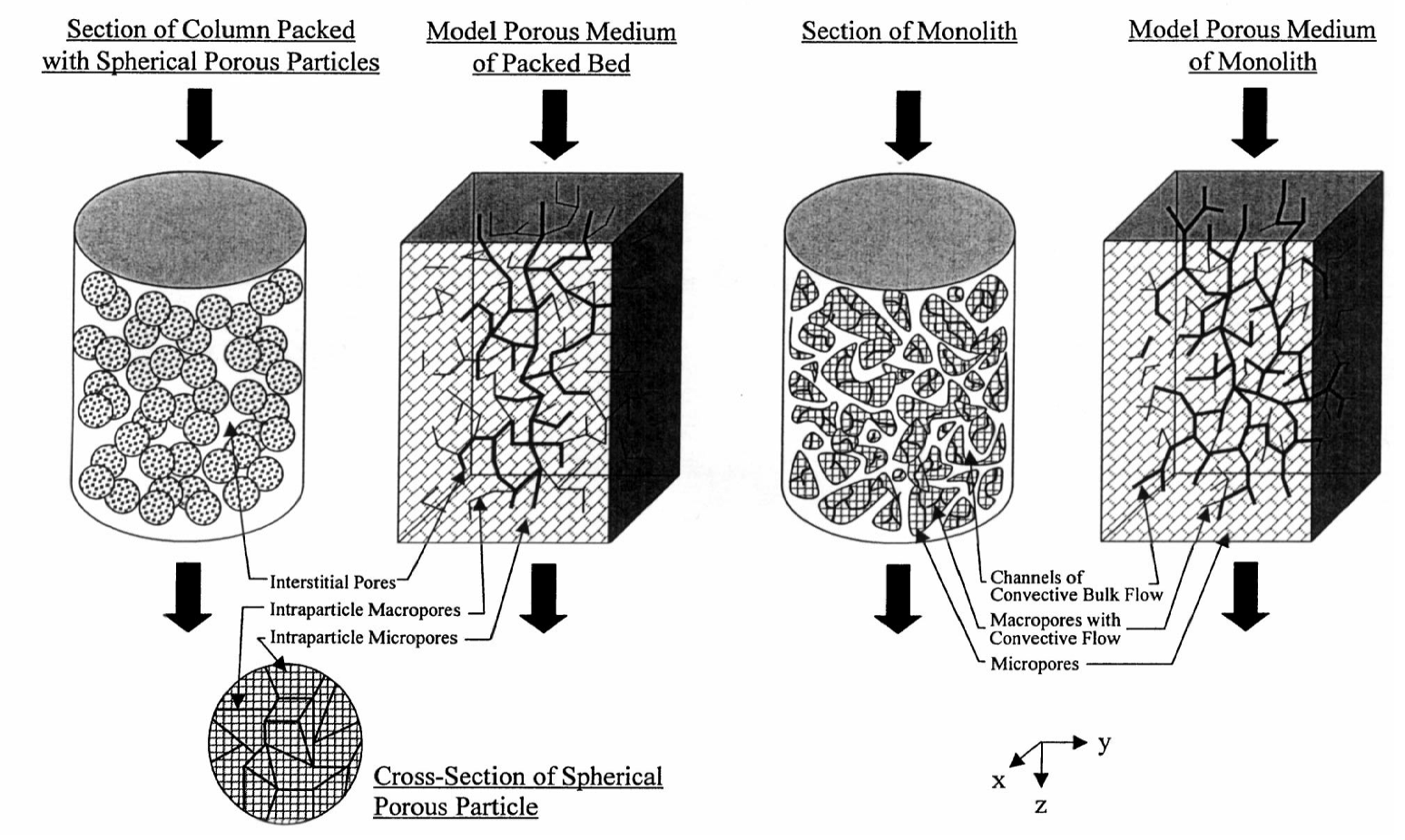

Fig. 1. Schematic representation through the pore network model of a finite small section of a packed bed and of a monolith (continuous bed).

correspond to the large pores of the monolith while the intraparticle pores in Fig. 1 correspond to the small and medium in size pores of the monolith. For all the simulations presented in this work, a lattice size of $15\times15\times15$ was used which, on previous experience with random networks [22,31–34], would be expected to provide a reasonably satisfactory representation of the pore network and does not require excessive computational times. The details of the construction of the lattice network and the computational methods employed in this work are presented in the reports of Meyers [31,32].

The functional form of the composite pore size distribution representing the porous structure and the value of the pore connectivity for the interstitial and intraparticle pores could be determined [22] from: (i) digital image analysis on scanning electron microscopy (SEM) images, (ii) transmission electron microscopy (TEM), (iii) mercury intrusion simulation and comparison of the results with experimental mercury intrusion data, (iv) size exclusion chromatography (SEC), and (v) studies involving adsorption capacity simulation and comparison of the results with experimental data. In the simulations of this work, the pore size distribution used in the work of Meyers and Liapis [22] is employed and its functional form is given by Eq. (1)

$$f(d)=\sum_{i=1}^{3}\frac{\gamma_i}{\sqrt{2\pi}\sigma_i}\exp\left(-\frac{1}{2}\left(\frac{d-\mu_i}{\sigma_i}\right)^2\right) \quad (1)$$

This pore size distribution is made up of the sum of three Gaussian distributions in order to represent the interstitial pores ($i=1$) in the column, the intraparticle macropores ($i=2$), and the intraparticle micropores ($i=3$). The values of γ_1, γ_2, and γ_3 in Eq. (1) are 0.013, 2.48, and 2.0 and represent the relative proportions of the interstitial pores, macropores, and micropores, respectively, in the packed column. The parameter d represents the pore diameter, μ_i ($i=1$, 2, 3) denotes the mean diameter of pores of class i, and σ_i ($i=1$, 2, 3) is the standard deviation of the diameter of pores of class i. The values of μ_i and σ_i in Eq. (1) are as follows: $\mu_1=4.40$ μm; $\mu_2=0.534$ μm; $\mu_3=0.039$ μm; $\sigma_1=1.30$ μm; $\sigma_2=0.38$ μm; and $\sigma_3=0.030$ μm. The values of the total porosity, ε_t, of the column, the void fraction, ε, of the bed, and the particle porosity, ε_p, are 0.68, 0.36, and 0.50, respectively. The diameter of the particles considered in this work is 15 μm and the ratio of μ_1 (mean pore size of interstitial pores) to particle diameter is $(4.40/15)=0.293$. Different investigators have found [35,36], by using various sphere packing models and mercury intrusion measurements, that the ratio of the mean diameter of the pores formed between the packed particles to the diameter of the particles is between 0.27–0.37 depending on the porosity of the packing. The ratio of $(4.40/15)=0.293$ utilized in this work is within the range of values reported in the literature. In this work, the pore size distribution functions for the intraparticle pores in Eq. (1) are considered to represent the distributions of the diameters of the pores within the matrix of the porous particles before the immobilization of the ligand molecules (active sites). When the ligand molecules are immobilized, the diameters of the intraparticle pores will become smaller than the diameters of the bare pores corresponding to Eq. (1). When the adsorbate molecules are adsorbed onto the immobilized ligand molecules (active sites), then the diameters of the intraparticle pores will decrease further. The effect of the size of the ligand and adsorbate molecules on the diameters of the intraparticle pores is considered in the following paragraphs of this section. It should be noted at this point that our pore network model formulation can use any physically and mathematically appropriate functional form for the pore size distribution *f(d)*. Loh and Wang [37] found that the functional form for the pore size distribution, *f(d)*, given by Eq. (1) could fit their pore size distribution data for the chromatographic particles examined in their work.

The pressure drop across a short cylindrical pore can be accurately determined to less than 1% in error by Eq. (2) which was constructed by Dagan et al. [38] for the pressure drop, Δp, through a cylindrical pore of finite length, l_p, under creeping flow conditions.

$$\Delta p=\left(\frac{16l_p}{\pi d}+3\right)\frac{8Q\mu}{d^3} \quad (2)$$

The diffusion rate of the molecules of species A having effective molecular radius α_1 through a single cylindrical pore of length l_p and radius r_p ($r_p=d/2$) is given by the following expression [22,39] when a

linear concentration gradient is considered to exist within the liquid in the pore and adsorption does not take place

$$J_{DA} = \pi r_p^2 K_A D_A \left(\frac{\Delta C_A}{l_p}\right) = P'_{DA}\left(\frac{\Delta C_A}{l_p}\right) = \pi r_p^2 P_{DA}\left(\frac{\Delta C_A}{l_p}\right) \quad (3)$$

where P'_{DA} denotes "permeance" = permeability(P_{DA}) × cross-sectional area. For certain chromatographic systems it is possible that, under certain conditions, the concentration gradient in the pore is nonlinear; in this case, one would have to integrate the material balance equation of the diffusing species for each pore. The total restriction to diffusion due to the combined effects of steric hindrance at the entrance to the pore and frictional resistance within the pore, may be considered (to a first approximation) to be provided by the expression proposed by Renkin [40], and the term $K_A D_A$ is given by

$$K_A D_A = D_{mf}\left(1 - \frac{\alpha_1}{r_p}\right)^2 \left[1 - 2.104\left(\frac{\alpha_1}{r_p}\right) + 2.09\left(\frac{\alpha_1}{r_p}\right)^3 - 0.95\left(\frac{\alpha_1}{r_p}\right)^5\right] = D_{mf}\varphi(r_p, \alpha_1) \quad (4)$$

where D_{mf} represents the free molecular diffusion coefficient of species A. Expressions for $K_A D_A$ with forms different than that given by Eq. (4) have been presented [41–45], but numerous calculations indicate that there are small differences between the results obtained from Eq. (4) and the expressions suggested in refs. [41–45].

The diffusion rate of species *A* through a serial combination of two cylindrical microscopic pores "*a*" and "*b*" whose lengths and pore radii are l_a, r_{pa}, l_b and r_{pb} ($r_{pa} \neq r_{pb}$), respectively, is given by the following expression when the system conditions are the same as those considered in Eq. (3)

$$J_{DA} = \left[\frac{\pi D_{mf}}{\left(\frac{f_a}{r_{pa}^2 \varphi(r_{pa}, \alpha_1)}\right) + \left(\frac{f_b}{r_{pb}^2 \varphi(r_{pb}, \alpha_1)}\right)}\right] \left(\frac{\Delta C_A}{l_p}\right) \quad (5)$$

where $l_p = l_a + l_b$, $f_a = l_a / l_p$, and $f_b = l_b / l_p = 1 - f_a$.

In this work, each ligand molecule, *B*, having effective molecular radius β_1, is taken to represent one active site and is attached covalently to the surface of the pore wall. Systems with concentrated ligand are considered because such systems are of practical interest; in these systems the ligand may reasonably be considered to be smeared uniformly along the walls of the cylindrical pore and the thickness of the ligand layer is taken to be t_o ($t_o = 2\beta_1$ for a monolayer of ligand). The molecules of species A (adsorbate) diffuse in the pore liquid and are adsorbed onto available vacant ligand molecules. The fractional saturation of the active sites (ligands) may be obtained [46] by the adsorption isotherm,

$$\theta = F(C_A) \quad (6)$$

where C_A is the local concentration of species A in solution and $F(C_A)$ represents a thermodynamically consistent functional form that describes accurately the experimental equilibrium adsorption data. For a large number of adsorption systems [47–50] adsorption equilibrium may be taken to be instantaneous on the macroscopic diffusion time scale. But in certain biospecific adsorption systems [7,11,13–20,49,51–58] the time constant of the adsorption step is comparable to the time constant of the diffusion mechanism, and thus, in these systems the adsorption step may not be considered as occurring infinitely fast. In such cases instantaneous adsorption may not be considered, and the value of θ, in such systems, should be obtained from a dynamic adsorption model that describes satisfactorily the dynamics of the adsorption step (mechanism), as shown in [52,53,55–58] where dynamic kinetic models have been constructed and used to describe the dynamics of the adsorption mechanism in systems where the adsorption step is not instantaneous and both the dynamics of the diffusion and adsorption mechanisms have to be considered.

A reasonable estimate of the adsorbate obstruction effect can be obtained by considering the adsorbate also to be uniformly smeared into a layer of thickness, t. The estimate is expected to be an underestimate of the real effect at low values of θ ($\theta << 1$), but becomes increasingly more realistic as $\theta \to 1$. Accordingly, the "*t* approach" [39] is worth study-

ing in detail. If r_p represents the bare pore radius, r_B denotes the radius of the pore with attached ligand, and r_{AB} corresponds to the radius of the pore with ligand and adsorbate, we have

$$r_B = r_p - t_o \tag{7}$$

$$r_{AB} = r_B - t \tag{8}$$

The diffusion rate of species A, J_{DA}, is then given by the following expression:

$$J_{DA} = \pi r_{AB}^2 P_{DA}\left(\frac{\Delta C_A}{l_p}\right) = \pi(r_B - t)^2 D_{mf}\varphi(r_{AB}, \alpha_1)\left(\frac{\Delta C_A}{l_p}\right) \tag{9}$$

The thickness of the adsorbed layer, t, is calculated [39] by Eq. (10)

$$t^2 - 2tr_B + 2r_B\gamma\theta\bar{V}_A = 0 \tag{10}$$

where

$$\gamma = \left(\frac{1}{\pi(\alpha_1)^2}\right) \quad \text{when } \alpha_1 > \beta_1 \tag{11a}$$

$$\gamma = \left(\frac{1}{\pi(\beta_1)^2}\right) \quad \text{when } \beta_1 > \alpha_1 \tag{11b}$$

and $\bar{V}_A$ is the molecular volume of the adsorbate. Thus, t can be obtained as a function of C_A and r_B by using Eqs. (6) and (10).

In the dilute adsorbate region ($\theta << 1$) Eqs. (8)–(10) would underestimate, as discussed above, the adsorbate obstruction effect. While the region of $\theta << 1$ may not be of practical interest, it is worth presenting the expressions that could be used to obtain a more realistic estimate of the adsorbate obstruction effect in the dilute adsorbate region ($\theta << 1$). The number of occupied ligands, n_B, within a pore of length l_p and radius $r_B = r_p - t_o$ is

$$n_B = 2\pi r_B l_p \gamma\theta \tag{12}$$

and the total length of obstructed pore, l_B, is approximately given by

$$l_B = n_B(2\alpha_1) = 4\pi r_B l_p \gamma\theta\alpha_1 \tag{13}$$

assuming that each adsorbed molecule obstructs a length of pore equal to $2\alpha_1$. The diffusion rate of species A, J_{DA}, is now given to a first approximation by the expression

$$J_{DA} = \left[\frac{\pi D_{mf}}{\left(\frac{f_A}{r_B^2\varphi(r_B, \alpha_1)}\right) + \left(\frac{f_B}{r_{pB}^2\varphi(r_{pB}, \alpha_1)}\right)}\right]\left(\frac{\Delta C_A}{l_p}\right) \tag{14}$$

where

$$f_A = \frac{l_A}{l_p}, \quad l_A = l_p - l_B, \quad f_B = \frac{l_B}{l_p} = 1 - f_A$$

and the effectively open portion of the cross-section of the partially obstructed pore is represented by an inscribed circle [39] of radius

$$r_{pB} = r_B - \alpha_1 = r_p - t_o - \alpha_1 \tag{15}$$

The reader will note that the above choices for l_B and especially for r_{pB} tend to produce an upper limiting estimate of the pore obstruction effect. An effective r_{pB} value based on the actual total unblocked pore cross-sectional area, namely

$$r_{pB} = ((r_p - t_o)^2 - \alpha_1^2)^{1/2} = (r_B^2 - \alpha_1^2)^{1/2} \tag{16}$$

would constitute the corresponding lower limiting estimate. For $\alpha_1 \ll r_B$, it makes little difference which value of r_{pB} is used. For $\alpha_1 \to (1/2)r_B$, however, Eq. (15) is obviously the realistic one, in view of the fact that much of the open cross-sectional area cannot be utilized by a diffusing molecule and the pore is effectively blocked ($P_{DA} \to 0$), as soon as $\alpha_1 > (1/2)r_B$. Note that, in the case of reversible adsorption such a pore is not completely blocked; because a molecule adsorbed at the pore entrance can desorb and move to the next adsorption site, thus opening the way for another adsorbate molecule to enter the pore. However, such ''single-file diffusion'' is slow. Thus, one can reasonably assume $P_{DA} = 0$, while the pore can still attain the proper C_A and θ values at equilibrium. It is worth mentioning that in Eqs. (12)–(16) the radius r_B is determined from Eq. (7) while the value of γ is obtained from Eq. (11a) or Eq. (11b) depending on the relative size of the molecular radii α_1 and β_1.

In certain adsorption systems where the volume $\bar{V}_B$ of the active site (ligand) could be considered to

be negligible (e.g., the active sites on the surface of the pores of anion and cation exchangers where $\bar{V}_B \cong 0$) the effective molecular radius, β_1, of the active site is taken to be approximately equal to zero, and therefore, in this case the thickness, t_o, of the ligand layer in Eqs. (7)–(16) is set equal to zero.

In the following subsections, the quantitative expressions and methods for determining the intraparticle velocity and the pore diffusion coefficient of the adsorbate molecules in the porous adsorbent particles or in monoliths under retained conditions, through the use of the pore network model constructed in this work, are presented.

2.1. Determination of the intraparticle fluid velocity

A pore in the pore network model is connected through nodes i and j, and thus, the flow rate Q_{ij} through each pore of length $l_{p,ij}$ in the network model can be obtained from Eq. (2) as follows:

$$Q_{ij} = \frac{(p_i - p_j)(d_{AB,ij})^3}{\left[\left(\frac{128 l_{p,ij}}{\pi d_{AB,ij}} + 24\right)\mu\right]} \tag{17}$$

For the ''*t* approach'', the diameter $d_{AB,ij}$ in Eq. (17) is determined by the expression

$$d_{AB,ij} = 2r_{AB,ij} = 2(r_{B,ij} - t_{ij}) = 2(r_{p,ij} - t_o - t_{ij}) \tag{18}$$

where $r_{p,ij}$ represents the radius of the bare pore connecting nodes *i* and *j*, and t_{ij} represents the thickness of the adsorbed layer in the pore of length $l_{p,ij}$ connecting nodes *i* and *j*; the value of t_{ij} for each pore of length $l_{p,ij}$ in the pore network is determined from Eq. (10). In our pore network model, the pore length, $l_{p,ij}$, was assigned to be equal to the diameter, $2r_{p,ij}$, of the bare pore and this assignment is considered to be topologically reasonable in light of the findings reported in the literature [22,37,59–61].

In the dilute adsorbate region ($\theta << 1$), the diameter $d_{AB,ij}$ in Eq. (17) is obtained from the following expression

$$d_{AB,ij} = 2r_{AB,ij} = 2\left[\left(\frac{l_{A,ij}}{l_{p,ij}}\right)r_{B,ij}^2 + \left(\frac{l_{B,ij}}{l_{p,ij}}\right)r_{pB,ij}^2\right]^{1/2} \tag{19}$$

where

$$l_{A,ij} = l_{p,ij} - l_{B,ij} \tag{20}$$

$$l_{B,ij} = 4\pi r_{B,ij} l_{p,ij} \gamma\theta\alpha_1 \tag{21}$$

$$r_{B,ij} = r_{p,ij} - t_o \tag{22}$$

$$r_{pB,ij} = r_{B,ij} - \alpha_1 = r_{p,ij} - t_o - \alpha_1 \tag{23a}$$

or

$$r_{pB,ij} = (r_{B,ij}^2 - \alpha_1^2)^{1/2} = ((r_{p,ij} - t_o)^2 - \alpha_1^2)^{1/2} \tag{23b}$$

Eq. (23a) produces, as discussed above (see Eq. (15)), an upper limiting estimate of the pore obstruction effect, while Eq. (23b) provides the corresponding lower limiting estimate, as mentioned above (see Eq. (16)). For $\alpha_1 \ll r_{B,ij}$, it makes little difference which value of $r_{pB,ij}$ is used. For $\alpha_1 \rightarrow (1/2)r_{B,ij}$, however, Eq. (23a) is obviously the realistic one.

The nodal pressures are obtained from the solution of a set of linear Eqs. that are constructed by rewriting Eq. (17) in terms of the net mass flow at node *i* [22,31,32]. Since all the flow on the top surface (first layer of nodes which is perpendicular to the direction of mass transfer) goes through the first layer of pores of the network, the nodes on the top surface can be reduced to one node whose net mass flow at the node is equal to the total mass flow. Similarly for the bottom surface, since all the flow exits the network onto the bottom surface, this surface can be reduced to one node whose net mass flow is the negative of the total. Lastly, for every interior node, since mass is conserved, the net mass flow is equal to zero. After the solution of the background pressures has been obtained, the pressure drop through the interstitial pore cluster of the network is determined, and thus, the amount of flow, Q_i, through the interstitial pores is calculated. Then the amount of intraparticle flow, Q_p, through the porous structure of the particles is obtained by subtracting the amount of flow through the interstitial pores from the total flow, Q_t, through the bed ($Q_p = Q_t - Q_i$). By letting $Q_t = V_{b,sup} S_c$ and $Q_p = \nu_{p,sup} S_c(1-\epsilon)$ (where S_c is the cross-sectional area of the column, $V_{b,sup}$ denotes the superficial velocity of the fluid in the column, and $\upsilon_{p,sup}$ represents the

superficial intraparticle velocity), the ratio of the superficial intraparticle fluid velocity to the superficial velocity of the fluid in the column is given by the following expression:

$$\frac{v_{p,sup}}{V_{b,sup}} = \left(\frac{1}{1-\varepsilon}\right)\left[\frac{Q_p}{Q_t}\right] \tag{24}$$

The ratio of the intraparticle interstitial velocity, $v_{p,i}$ ($v_{p,i} = v_{p,sup}/\varepsilon_p$), to the interstitial bed velocity, $V_{b,i}$ ($V_{b,i} = V_{b,sup}\varepsilon$), could provide more useful practical information when one considers to compare the relative speeds of movement of the solute inside the pores of the particle due to intraparticle fluid flow and pore diffusion. The ratio of $v_{p,i}$ to $V_{b,i}$ is as follows:

$$\frac{v_{p,i}}{V_{b,i}} = \left(\frac{\varepsilon}{\varepsilon_p}\right)\left[\frac{v_{p,sup}}{V_{b,sup}}\right] = \left(\frac{\varepsilon}{\varepsilon_p(1-\varepsilon)}\right)\left[\frac{Q_p}{Q_t}\right] \tag{25}$$

By employing Eqs. (17)–(23b) in the pore network model developed in this work, the values of $v_{p,sup}/V_{b,sup}$ and $v_{p,i}/V_{b,i}$ are obtained for different values of loading, θ, during the adsorption of the adsorbate molecules onto the immobilized active sites (ligands).

2.2. Determination of the intraparticle pore diffusivity

The basic expression for the mass flux, $N_{DA,ij}$, of the adsorbate molecules *A* through a cylindrical pore of length $l_{p,ij}$ can be employed in order to determine the concentration difference through the pore connected to nodes *i* and *j*. The expression for $N_{DA,ij}$ is given by Eq. (26)

$$\begin{aligned} N_{DA,ij} &= \frac{J_{DA,ij}}{\pi(r_{AB,ij})^2} = (K_A D_A)_{ij}\left(\frac{C_{A,i} - C_{A,j}}{l_{p,ij}}\right) \\ &= D_{mf}\varphi(r_{AB,ij}, \alpha_1)\left(\frac{C_{A,i} - C_{A,j}}{l_{p,ij}}\right) \end{aligned} \tag{26}$$

For the ''*t* approach'', the radius, $r_{AB,ij}$, in Eq. (26) is determined by the expression

$$r_{AB,ij} = r_{B,ij} - t_{ij} = r_{p,ij} - t_o - t_{ij} \tag{27}$$

The value of the thickness, t_{ij}, of the adsorbed layer for each pore of length $l_{p,ij}$ in the pore network is determined from Eq. (10).

In the dilute adsorbate region ($\theta \ll 1$), the radius, $r_{AB,ij}$, in Eq. (26) is obtained from the following expression:

$$r_{AB,ij} = \left[\left(\frac{l_{A,ij}}{l_{p,ij}}\right)r_{B,ij}^2 + = \left(\frac{l_{B,ij}}{l_{p,ij}}\right)r_{pB,ij}^2\right]^{1/2} \tag{28}$$

The values of $l_{A,ij}$, $l_{B,ij}$, $r_{B,ij}$, and $r_{pB,ij}$ in Eq. (28) are determined from Eqs. (20)–(23b).

For a three-dimensional network of cylindrical pores (as is the network used in this work), it is more convenient to write expressions for the net flux at each node in order to calculate the nodal concentrations. Since the mass flux given on the top surface (first layer of nodes which is perpendicular to the direction of the net mass transfer) of the network is the same as the sum of the mass fluxes of the pores emanating from this surface into the network, the top layer of nodes can be reduced to a single node (node 1). The net mass flux between this node and all the nodes of the second layer is equal to the specified total mass flux, N_{DAo}, and is given by the following expression

$$\begin{aligned} \sum_{j=1}^{N_a} N_{DA,1j} &= \sum_{j=1}^{N_a} (K_A D_A)_{1j}\left(\frac{C_{A,1} - C_{A,j}}{l_{p,1j}}\right)\delta_j \\ &= \sum_{j=1}^{N_a} (D_{mf}\varphi(r_{AB,1j}, \alpha_1))\left(\frac{C_{A,1} - C_{A,j}}{l_{p,1j}}\right)\delta_j \\ &= N_{DAo} \end{aligned} \tag{29}$$

where N_{DAo} is the flux specified (set) at node 1, N_a represents the total number of nodes in the cubic lattice network, and δ_j is equal to one when an adjacent node is connected by a pore (bond) to node 1 while δ_j is equal to zero when an adjacent node is not connected by a pore to node 1. Similarly, the bottom surface of the network can be reduced to a single node (node N_e) where the sum of the mass fluxes emanating from the last layer of nodes of the network to node N_e is equal to the negative of the total specified mass flux, N_{DAo}, and is given by the expression

$$\begin{aligned} \sum_{j=1}^{N_a} N_{DA,N_e j} &= \sum_{j=1}^{N_a} (K_A D_A)_{N_e j}\left(\frac{C_{A,N_e} - C_{A,j}}{l_{p,N_e j}}\right)\delta_j \\ &= \sum_{j=1}^{N_a} (D_{mf}\varphi(r_{AB,N_e j}, \alpha_1))\left(\frac{C_{A,N_e} - C_{A,j}}{l_{p,N_e j}}\right)\delta_j \\ &= -N_{DAo} \end{aligned} \tag{30}$$

where δ_j is equal to one when an adjacent node is connected by a bond (pore) to node N_e while δ_j is equal to zero when an adjacent node is not connected by a pore to node N_e. Then, for every interior node (nodes on the second through the fifteenth layers, where a layer is the plane surface perpendicular to the net mass flux direction) the net mass flux must be equal to zero, as shown in Eq. (31)

$$\sum_{j=1}^{N_a} N_{DA,ij} = \sum_{j=1}^{N_a} (K_A D_A)_{ij} \left(\frac{C_{A,i} - C_{A,j}}{l_{p,ij}} \right) \delta_j = \sum_{j=1}^{N_a} (D_{mf} \varphi(r_{AB,ij}, \alpha_1)) \left(\frac{C_{A,i} - C_{A,j}}{l_{p,ij}} \right) \delta_j = 0 \quad (31)$$

where δ_j is equal to one when node i is connected to adjacent node j by a pore (bond) while δ_j is equal to zero when node i is not connected by a pore to adjacent node j. The simultaneous solution of Eqs. (29)–(31) provides the value of the concentration of species A at each node of the network. In order to determine the pore diffusivity, D_p, of species A in the model porous medium, the total permeability, P, of species A in the model porous medium must first be calculated. The total permeability, P, is calculated from Eq. (32)

$$P = \left(\frac{1}{2} \right) \left(\frac{1}{S_o} \right) \left[\sum_{i=1}^{N_a} \sum_{j=1}^{N_a} P'_{DA,ij} \left(\frac{\Delta c_{A,ij}}{V_{ij}} \right) \right] \quad (32)$$

where N_a represents the total number of nodes in the network; $P'_{DA,ij} = \pi (r_{AB,ij})^2 (K_A D_A)_{ij} = \pi (r_{AB,ij})^2 (D_{mf} \varphi(r_{AB,ij}, \alpha_1))$; V_{ij} represents the ratio of the pore length $l_{p,ij}$ to the shortest distance connecting node i with another adjacent node; S_o is the cross-sectional area of the model porous medium whose pores are intraparticle pores; and $\Delta c_{A,ij}$ represents the normalized concentration difference where

$$c_{A,i} = \frac{(C_{A,i} - C_{A,N_e})}{(C_{A,1} - C_{A,N_e})}; \qquad c_{A,1} = 1; \qquad c_{A,N_e} = 0 \quad (33)$$

The factor $\frac{1}{2}$ in Eq. (32) allows for counting each capillary twice in the summation. Also, although there are concentration gradients through pores on the plane (x, y) perpendicular to the direction (z) of net mass transfer, it is the pores in the z direction which contribute to the net flux. For this reason, Eqs. (29)–(31) are solved for all nodes in the network of intraparticle pores taking into account all intraparticle pores so as to determine a concentration gradient for each pore, while Eq. (32) is calculated for all nodes taking into account only the pores in the direction (z) of net mass transfer.

The pore diffusion coefficient, D_p, of the molecules of species A in the porous medium is then obtained from Eq. (34)

$$D_p = \frac{P}{\varepsilon_p} \quad (34)$$

where the value of P is determined from Eq. (32). By employing Eqs. (26)–(33) in the pore network model developed in this work, the value of the pore diffusion coefficient, D_p, of the adsorbate molecules A is determined from Eq. (34) for different values of loading, θ, during the adsorption of species A onto the immobilized ligands (active sites).

3. Results and discussion

The results presented in this work are obtained from the pore network model for the case where all the intraparticle macropores with pore diameter greater than 1 μm are not randomly distributed relative to the other intraparticle pores, and are added through a random network connected with a high frequency to the pore cluster of the interstitial pores; this case would represent porous particles having on their outer surface a higher incidence of macropores which could permeate into the interior of the porous particles. Chromatographic particles whose pore network would have the structure of the porous medium discussed above, would better facilitate intraparticle fluid flow and diffusion than porous particles whose structure is such that their intraparticle macropores of all sizes are randomly distributed relative to the micropores [22,31,32]. Simulation of the model porous medium using the pore size distribution given in Eq. (1) yields a percolation threshold at pore connectivity of 2.6 ($n_T = 2.6$). Connectivities below this value do not produce a percolating cluster of interstitial pores necessary for flow through the model porous bed. In this work, results are presented for values of the pore connectivity higher than 2.6. When n_T is equal to 6, the lattice network is completely occupied, since, in this

case, the value of n_T is equal to the coordination number of the cubic lattice.

In this study, the adsorbate is taken to be β-galactosidase and two different kinds of adsorption sites are considered. In one case, the adsorbate is adsorbed on the surface of the pores of an ion-exchanger. In another case, the β-galactosidase is adsorbed onto anti-β-galactosidase molecules immobilized on the surface of the pores of the chromatographic particles. In the case of the ion-exchanger, the thickness t_o of the layer of active sites is taken to be approximately equal to zero ($t_o \cong 0$). In the case of affinity chromatography, the thickness t_o of a monolayer of ligand (a monolayer formed from anti-β-galactosidase molecules) is taken to be equal to $2\beta_1$ ($t_o = 2\beta_1$) where β_1 represents the effective molecular radius of anti-β-galactosidase. The effective molecular radii of β-galactosidase and anti-β-galactosidase are denoted by α_1 and β_1, respectively, and their values are as follows: $\alpha_1 = 70.6$ Å and $\beta_1 = 47.7$ Å. The value of the free molecular diffusivity of β-galactosidase is 3.90×10^{-11} m^2/s, and the value of the porosity ε_p of the porous medium is equal to 0.50 when the thickness t_o of the layer of active sites is equal to zero. Adsorbent I is taken to represent the porous ion-exchange particles while the chromatographic particles with the immobilized anti-β-galactosidase are represented by Adsorbent II. In this work, the superficial fluid velocity in the column, $V_{b,sup}$, has been taken to be 1000 cm/h which corresponds to an interstitial fluid velocity in the column, $V_{b,i}$, of 2777.77 cm/h.

In Fig. 2, the ratios of the intraparticle interstitial velocities $v_{pu,i}$ ($t_o = 0$, $t = 0$) and $v_{put_o,i}$ ($t_o = 2\beta_1$, $t = 0$) to the interstitial column fluid velocity, $V_{b,i}$, versus the pore connectivity, n_T, are presented for the intraparticle convective flow of β-galactosidase in Adsorbents I and II under unretained conditions.

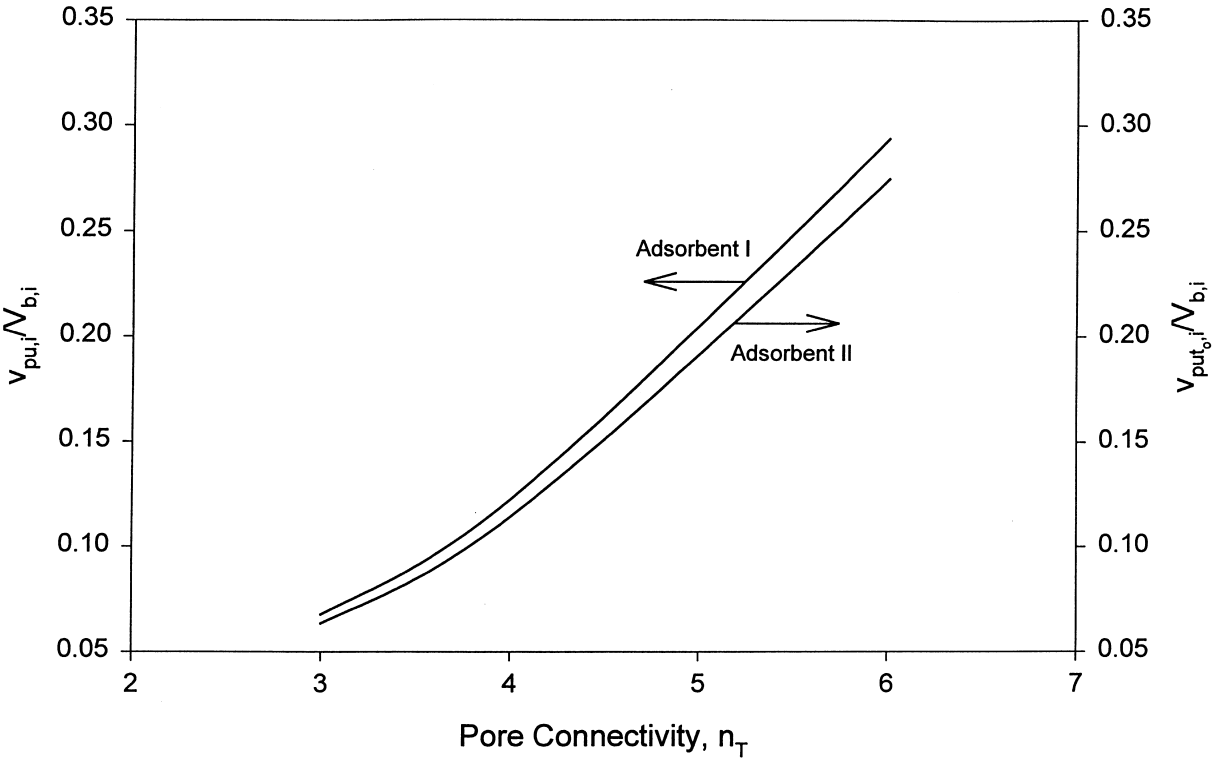

Fig. 2. Ratios of the intraparticle interstitial velocities, $v_{pu,i}$ ($t_o = 0$, $t = 0$) and $v_{put_o,i}$ ($t_o = 2\beta_1$, $t = 0$) to the interstitial fluid velocity in the column, $V_{b,i}$, under unretained conditions in Adsorbents I and II, respectively, versus the pore connectivity, n_T, of the porous medium. Curve for Adsorbent I: $t_o = 0$ and $t = 0$; Curve for Adsorbent II: $t_o = 0.00954$ μm and $t = 0$.

The results in Fig. 2 indicate that the values of the ratios $v_{pu,i}/V_{b,i}$ and $v_{put_o,i}/V_{b,i}$ increase significantly as the pore connectivity, n_T, of the intraparticle pores increases. It can also be observed that the intraparticle interstitial velocity in Adsorbent II is slightly smaller than the intraparticle interstitial velocity in Adsorbent I due to the obstruction effect resulting from the immobilized layer of the anti-β-galactosidase molecules; the largest percentage difference between $v_{pu,i}/V_{b,i}$ and $v_{put_o,i}/V_{b,i}$ is 6.48% and occurs when $n_T=6.0$ (when n_T is equal to 6.0, the lattice network is completely occupied, since, in this case, the value of n_T is equal to the coordination number of the cubic lattice), while the smallest percentage difference is 6.27% and occurs at $n_T=3.0$. The results in Fig. 2 indicate that the effect of the layer of immobilized ligands on the intraparticle interstitial velocity is rather small, while the effect of the value of the pore connectivity, n_T, on the intraparticle interstitial velocity is very large.

In Figs. 3 and 4 the ratios of the intraparticle interstitial velocities $v_{pr,i}$ ($t_o=0$, $t>0$) and $v_{prt_o,i}$ ($t_o=2\beta_1$, $t>0$) to the interstitial column fluid velocity, $V_{b,i}$, versus the fractional saturation of active sites, θ, are presented for the intraparticle convective flow of β-galactosidase in Adsorbents I and II, respectively, under retained conditions and for different values of the pore connectivity, n_T. The results in Figs. 3 and 4 indicate that the values of the ratios $v_{pr,i}/V_{b,i}$ and $v_{prt_o,i}/V_{b,i}$ increase substantially as the pore connectivity, n_T, of the intraparticle pores increases. The results also show that the values of $v_{pr,i}/V_{b,i}$ and $v_{prt_o,i}/V_{b,i}$ are insignificantly affected by the increase in the value of θ (this is not the case when the effect of θ on the effective pore diffusion coefficient of β-galactosidase is considered, as the results in Figs. 6 and 7 indicate). In the ''t approach'', the thickness, t, of the adsorbed layer is a function of α_1, β_1, γ, θ, and of the pore radius r_p, as Eqs. (7)–(11b) indicate. For pores of larger radii, the

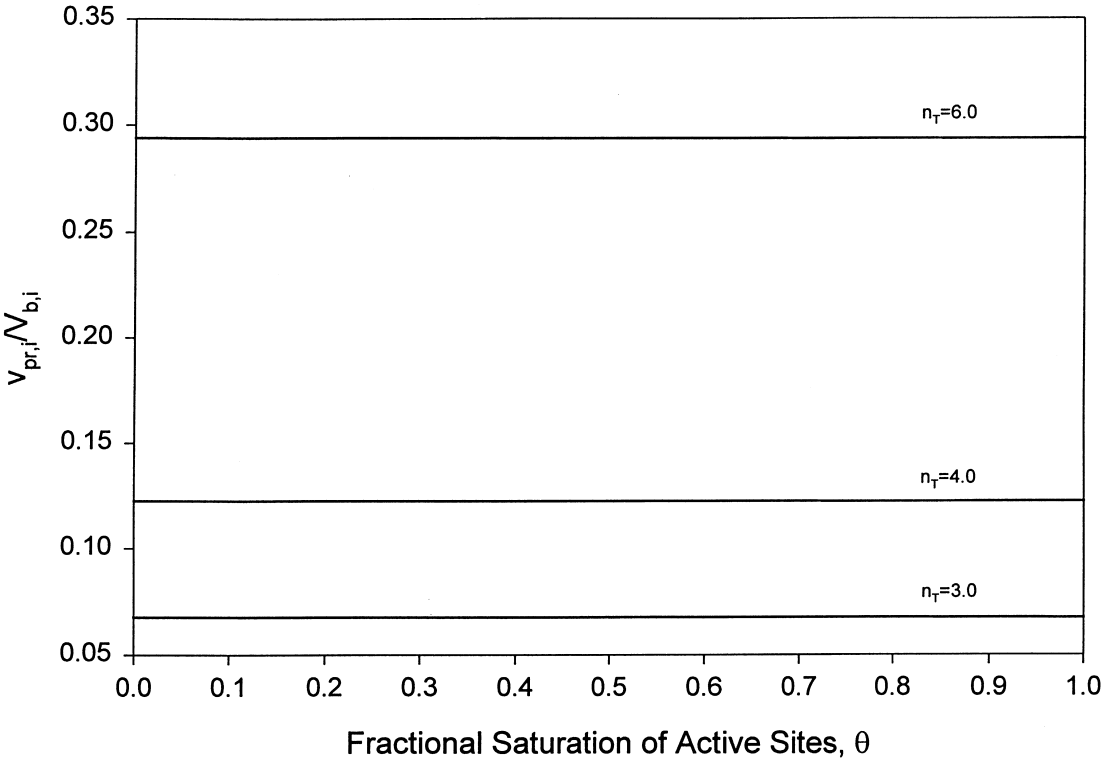

Fig. 3. Ratio of the intraparticle interstitial velocity, $v_{pr,i}$ under retained conditions in Adsorbent I ($t_o=0$, $t>0$) to the interstitial fluid velocity in the column, $V_{b,i}$, versus the fractional saturation of active sites, θ, and for different values of the pore connectivity, n_T.

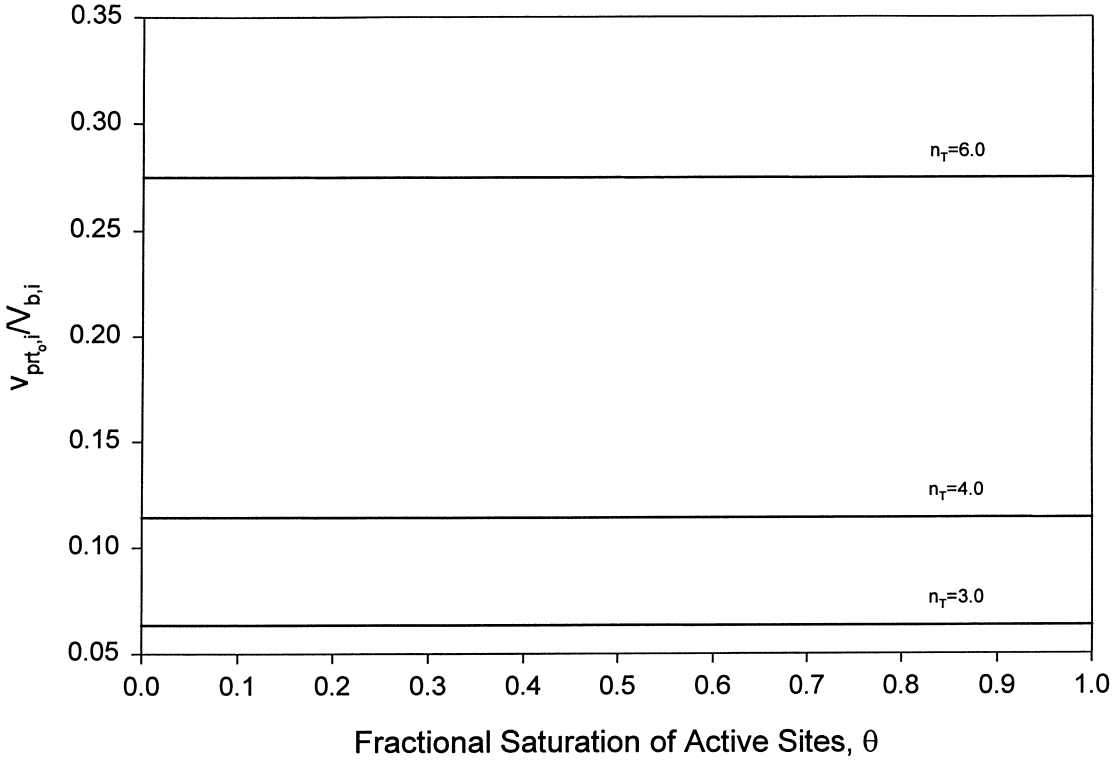

Fig. 4. Ratio of the intraparticle interstitial velocity $v_{prt_o,i}$ under retained conditions in Adsorbent II ($t_o=2\beta_1$, $t>0$) to the interstitial fluid velocity in the column, $V_{b,i}$, versus the fractional saturation of active sites, θ, and for different values of the pore connectivity, n_T.

value of the thickness, t, of the adsorbed layer is smaller and with increasing values of θ, the radius of the pore is almost unaffected. Since most of the intraparticle fluid flow occurs in the pores of larger radii, the values of the ratios $v_{pr,i}/V_{b,i}$ and $v_{prt_o,i}/V_{b,i}$ are almost unaffected with increasing values of θ. The contribution of pores of smaller radii to the intraparticle fluid flow is very small (insignificant) and many pores of small radii become blocked with increasing values of θ. By comparing the results in Figs. 2–4, one could observe that the effect of the value of t_o on the intraparticle interstitial velocity may be slightly more pronounced than the effect of the thickness, t, of the adsorbed layer. A constant thickness t_o ($t_o=2\beta_1$) is subtracted from the radius of each pore (as shown in Eq. (7)), regardless of the value of the pore radius; thus, the thickness t_o could be substantially larger than the thickness, t, of the adsorbed layer in the pores of larger radii. Since most of the intraparticle fluid flow occurs in the pores of larger radii, the value of $t_o>0$ ($t_o=2\beta_1$, $\beta_1>0$) could have a slight obstruction effect on the intraparticle interstitial fluid flow, and this can be observed by comparing the results presented in Fig. 2 where for Adsorbent I the value of t_o is taken to be approximately equal to zero while for Adsorbent II the value of t_o is equal to 95.4 Å ($t_o=2\beta_1=2$(47.7 Å)=95.4 Å). In conclusion, the data in Figs. 2–4 indicate that for the adsorption systems studied in this work, the obstruction effects on the intraparticle interstitial velocity, due to (i) the thickness, t_o, of the immobilized active sites and (ii) the thickness, t, of the adsorbed layer (and therefore, due to the value of loading, θ), are small and appear to be insignificant when they are compared with the very significant effect that the value of the pore connectivity, n_T, has on the magnitude of the intraparticle interstitial velocity.

Thus, the results in Figs. 2–4 indicate that the pore network model could allow one to determine, for a

given porous medium of interest and for a given value of the interstitial column fluid velocity, $V_{b,i}$, the value of the intraparticle interstitial fluid velocity under retained or unretained conditions in an a priori manner. This is a very significant result and can be used to provide in an a priori manner numerical values for the intraparticle velocity components [13–20,22] which are utilized in the macroscopic models [13–20] that describe the dynamic behavior of chromatographic separations in packed columns. Furthermore, the results in Figs. 2–4 clearly indicate that porous particles with high pore connectivities should be used in chromatographic separations.

In Fig. 5, the ratios of the effective pore diffusion coefficients D_{pu} ($t_o=0$, $t=0$) and D_{put_o} ($t_o=2\beta_1$, $t=0$) to $\varepsilon_p D_{mf}$ versus the pore connectivity, n_T, are presented for the diffusion of β-galactosidase in Adsorbents I and II under unretained conditions. It can be observed that the increase in the values of the ratios $D_{pu}/\varepsilon_p D_{mf}$ and $D_{put_o}/\varepsilon_p D_{mf}$ with n_T in the range of values of n_T between 4.5 to 6, is significantly smaller than the increase in the values of $D_{pu}/\varepsilon_p D_{mf}$ and $D_{put_o}/\varepsilon_p D_{mf}$ with n_T in the range of values of n_T between 3.0 and 4.5. This result is due to the fact that the pores in the pore network are significantly more interconnected when n_T is in the range 4.5–6. The results in Fig. 5 clearly show that for a given value of n_T, the effective pore diffusion coefficient of β-galactosidase in Adsorbent II is substantially smaller than the effective pore diffusion coefficient of the adsorbate in Adsorbent I, and the difference in the values of D_{pu} and D_{put_o} increases as the value of the pore connectivity n_T decreases; these results indicate that the immobilized layer of anti-β-galactosidase in Adsorbent II reduces substantially the magnitude of the effective pore diffusion coefficient of β-galactosidase when compared with the magnitude of the effective pore diffusion coefficient

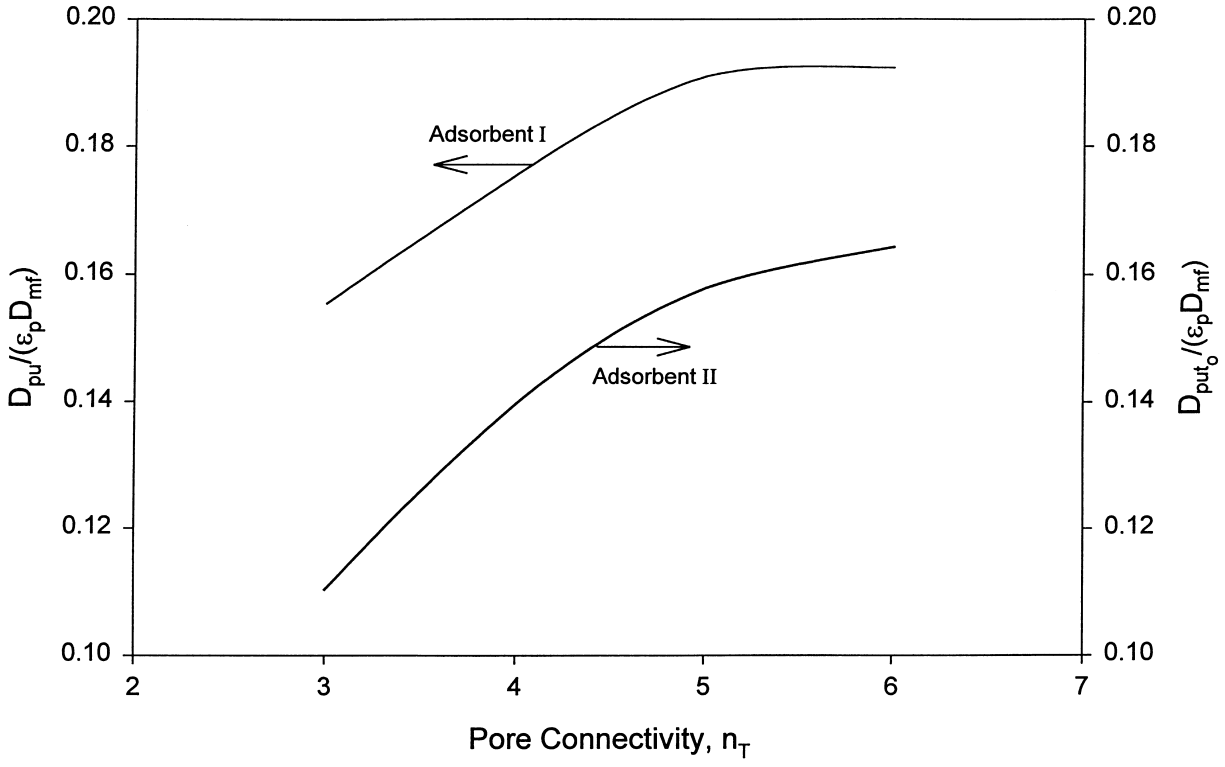

Fig. 5. Ratios of the effective pore diffusion coefficients D_{pu} ($t_o=0$, $t=0$) and D_{put_o} ($t_o=2\beta_1$, $t=0$) to $\varepsilon_p D_{mf}$ under unretained conditions in Adsorbents I and II, respectively, versus the pore connectivity, n_T, of the porous medium. Curve for Adsorbent I: $t_o=0$ and $t=0$; Curve for Adsorbent II: $t_o=0.00954$ μm and $t=0$.

of the adsorbate in the porous ion-exchange particles (Adsorbent I). The data in Fig. 5 indicate that porous particles with high pore connectivities should be employed, especially in affinity chromatography systems.

In Figs. 6 and 7, the ratios of the effective pore diffusion coefficients D_{pr} ($t_o=0$, $t>0$) and D_{prt_o} ($t_o=2\beta_1$, $t>0$) to $\varepsilon_p D_{mf}$ versus the fractional saturation of active sites, θ, are presented for the diffusion of β-galactosidase in Adsorbents I and II, respectively, under retained conditions and for different values of the pore connectivity, n_T. Figs. 6 and 7 show the decrease of the effective pore diffusion coefficient of β-galactosidase with increasing θ (all curves in Figs. 6 and 7) and t_o (for the same pore connectivity compare the results in Fig. 6 where $t_o=0$ with those in Fig. 7 where $t_o=2\beta_1$), for every value of the pore connectivity, n_T; in keeping with the fact that θ (through the value of t) and t_o determine the size of the obstructions in the path of diffusing molecules. However, Figs. 6 and 7 illustrate rather strikingly the important point that the magnitude of the obstruction effect depends on the pore connectivity, n_T, and that this dependence becomes increasingly more marked as θ and/or t_o increase. The value of the effective pore diffusion coefficient of β-galactosidase is always enhanced with increasing n_T, in view of the fact that a greater number of alternative diffusion pathways is thereby made available to the diffusing molecules, thus enabling them to bypass narrow pores (which at best have low permeability and at worst are completely blocked). The results in Figs. 6 and 7 clearly indicate that porous particles with high pore connectivities should be employed in adsorption systems involving large magnitudes of the fractional saturation of active sites, θ, particularly in affinity chromatography systems.

The results in Figs. 5–7 indicate that by employing the pore network modeling approach developed in this work, one does not need to estimate values for

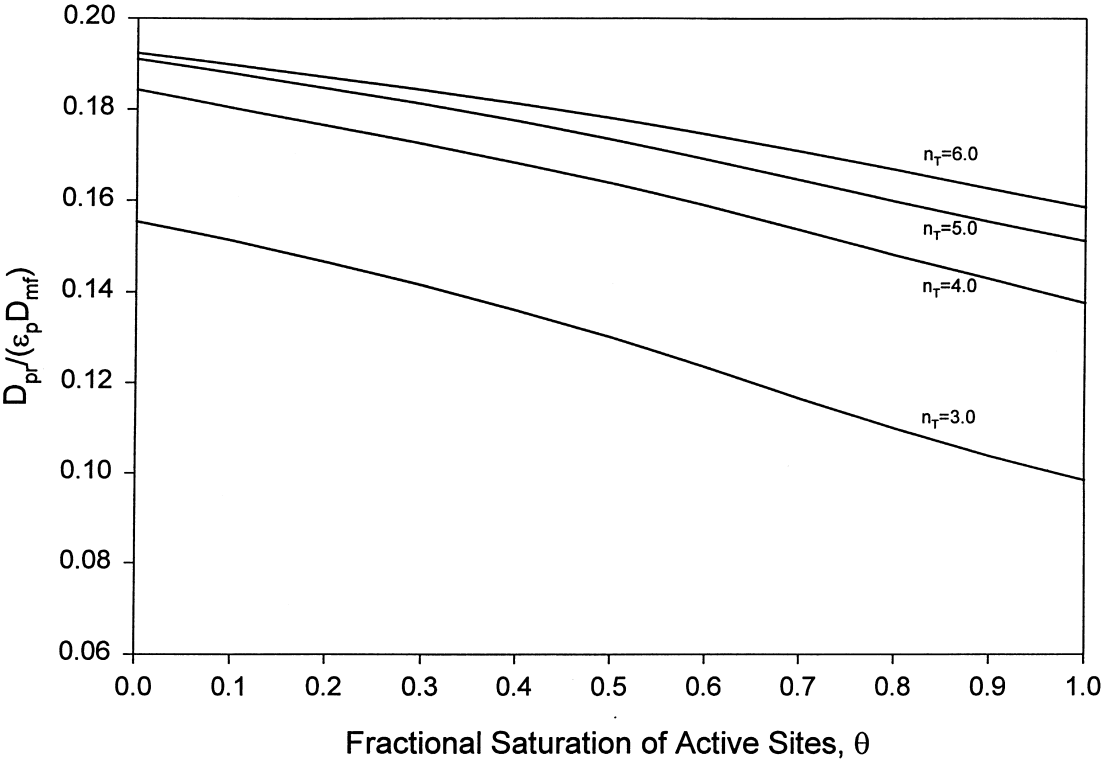

Fig. 6. Ratio of the effective pore diffusion coefficient D_{pr} under retained conditions in Adsorbent I ($t_o=0$, $t>0$) to $\varepsilon_p D_{mf}$ versus the fractional saturation of active sites, θ, and for different values of the pore connectivity, n_T.

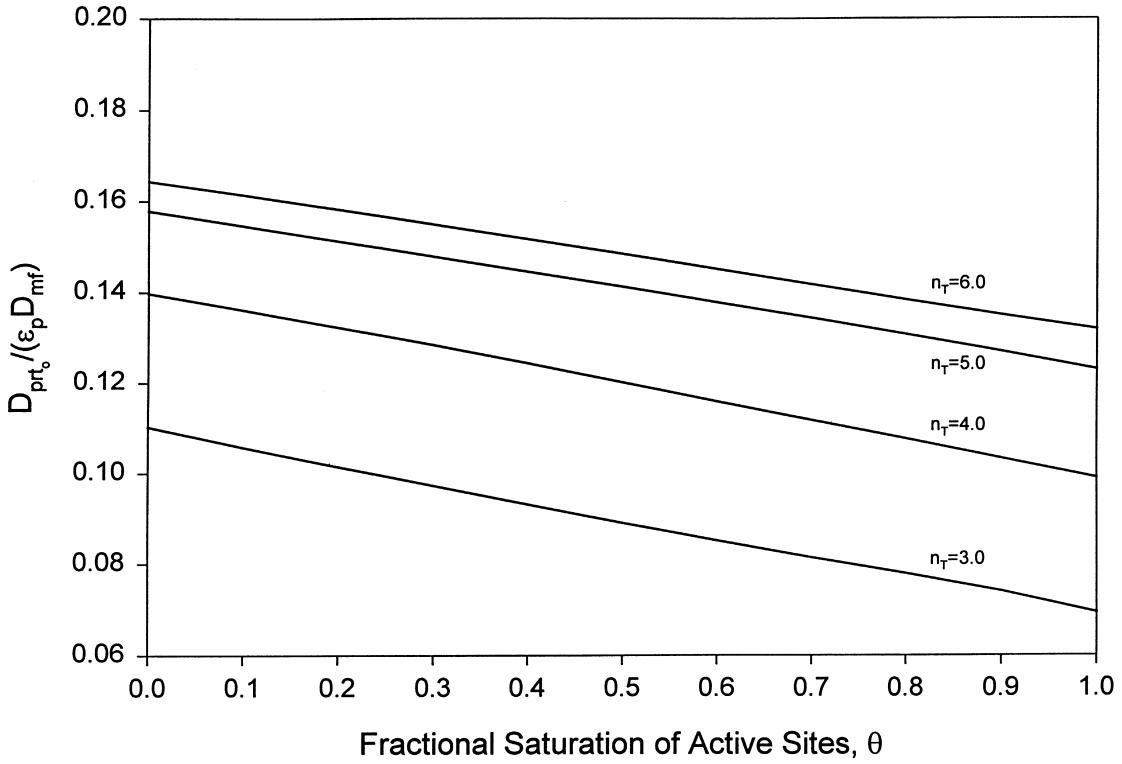

Fig. 7. Ratio of the effective pore diffusion coefficient D_{prt_o} under retained conditions in Adsorbent II ($t_o = 2\beta_1$, $t > 0$) to $\varepsilon_p D_{mf}$ versus the fractional saturation of active sites, θ, and for different values of the pore connectivity, n_T.

the empirical parameter of tortuosity since tortuous pathways for mass transfer are already built within the pore network model. Furthermore, the pore network model properly accounts for the overall restriction to diffusion due to (i) steric hindrance at the entrance to the pores, (ii) frictional resistance within the pores, (iii) obstruction by the immobilized active sites (ligands), and (iv) obstruction by the adsorbed molecules of the adsorbate. If one would consider the empirical relationship $D_p = (\varepsilon_p D_{mf})(\lambda/\tau)$ where D_p represents the effective pore diffusion coefficient of the adsorbate molecules in the porous particles, λ denotes the hindrance parameter of the porous medium and τ denotes the average tortuosity in the porous particles, then the ratios in the ordinates of Figs. 5–7 might be thought of as providing the value of the ratio λ/τ in an a priori manner. The results in Figs. 5–7 indicate that the pore network model can be used to provide in an a priori manner numerical results for the effective pore diffusion coefficient of the adsorbate molecules under unretained and retained conditions; these values of the effective pore diffusion coefficient could then be employed in the macroscopic models [13–20] that describe the dynamic behavior of chromatographic separations in monoliths (continuous beds) and in columns packed with porous particles.

In Fig. 8, the ratios of the intraparticle interstitial velocities $v_{pu,i}$ ($t_o = 0$, $t = 0$) and $v_{put_o,i}$ ($t_o = 2\beta_1$, $t = 0$) to their respective diffusion velocities $v_{DA,u}$ ($t_o = 0$, $t = 0$) and v_{DA,ut_o} ($t_o = 2\beta_1$, $t = 0$), versus the pore connectivity, n_T, are presented, for the intraparticle transport of β-galactosidase in Adsorbents I and II under unretained conditions. The diffusion velocities $v_{DA,u}$ and v_{DA,ut_o} could be estimated (Carlson and Dranoff [62]) from the ratios D_{pu}/R_p and D_{put_o}/R_p, respectively, where R_p represents the radius of the porous chromatographic particle; the value of R_p is 7.5 μm for the porous particles used here. It can be observed that the ratios

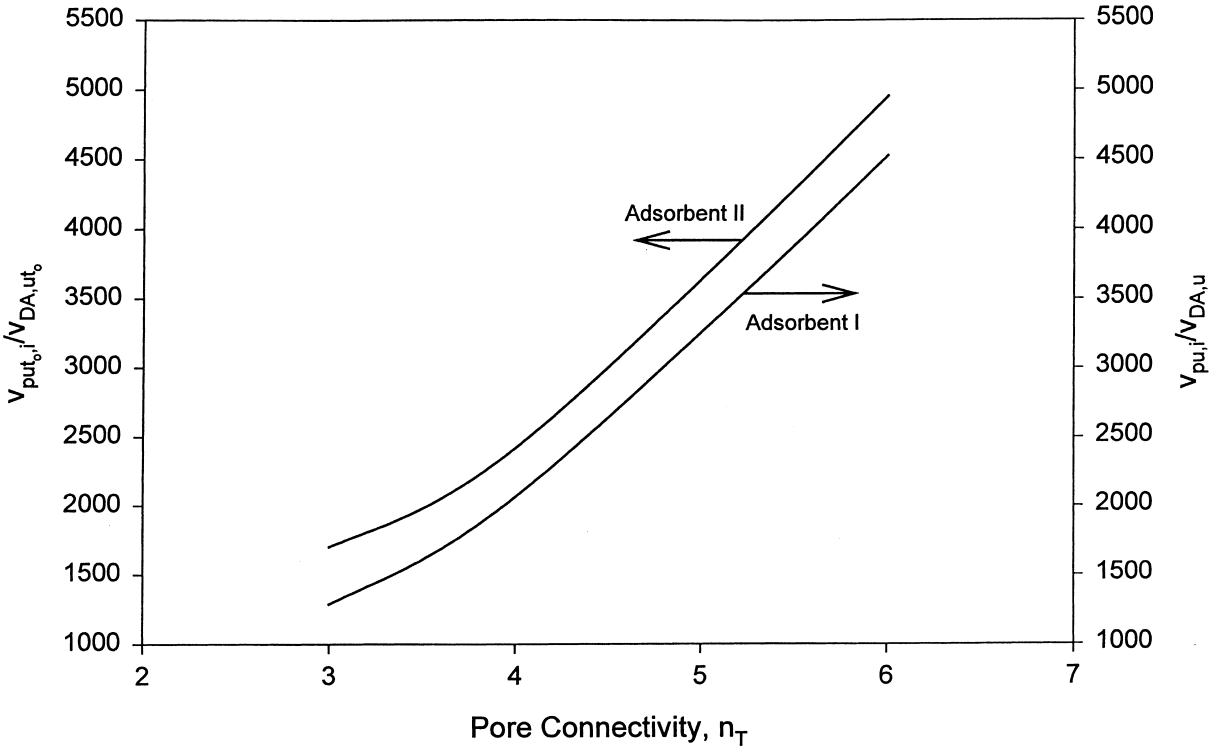

Fig. 8. Ratios of the intraparticle interstitial velocities $v_{pu,i}$ ($t_o = 0$, $t = 0$) and $v_{put_o,i}$ ($t_o = 2\beta_1$, $t = 0$) to their respective diffusion velocities $v_{DA,u}$ ($t_o = 0$, $t = 0$) and v_{DA,ut_o} ($t_o = 2\beta_1$, $t = 0$) under unretained conditions, versus the pore connectivity, n_T, of the porous medium. Curve for Adsorbent I: $t_o = 0$ and $t = 0$; Curve for Adsorbent II: $t_o = 0.00954$ μm and $t = 0$.

$v_{pu,i}/v_{DA,u}$ and $v_{put_o,i}/v_{DA,ut_o}$ increase significantly as the pore connectivity, n_T, increases. It can also be observed that even at low values of n_T the values of the intraparticle interstitial velocities $v_{pu,i}$ and $v_{put_o,i}$ are orders of magnitude larger than the diffusion velocities $v_{DA,u}$ and v_{DA,ut_o}, and this indicates that the intraparticle interstitial velocity can significantly enhance the speed of movement of the molecules of β-galactosidase inside the porous structure of the adsorbent particles. For a given value of n_T, the value of the ratio $v_{pu,i}/v_{DA,u}$ in Adsorbent I is smaller than the value of the ratio $v_{put_o,i}/v_{DA,ut_o}$ in Adsorbent II because the thickness, t_o, of the layer of immobilized anti-β-galactosidase molecules has an obstruction effect on the diffusion of β-galactosidase in Adsorbent II so that the value of v_{DA,ut_o} is smaller than the value of $v_{DA,u}$.

In Figs. 9 and 10 the ratios of $v_{pr,i}/v_{DA,r}$ ($t_o = 0$, $t > 0$) and $v_{prt_o,i}/v_{DA,rt_o}$ ($t_o = 2\beta_1$, $t > 0$) versus the fractional saturation of active sites, θ, are presented, respectively, for the intraparticle transport of β-galactosidase in Adsorbents I and II under retained conditions and for different values of the pore connectivity, n_T. Figs. 9 and 10 show the increase of the values of the ratios $v_{pr,i}/v_{DA,r}$ and $v_{prt_o,i}/v_{DA,rt_o}$ with increasing θ (all curves in Fig. 9 and 10) and t_o (for the same pore connectivity compare the results in Fig. 9 where $t_o = 0$ with those in Fig. 10 where $t_o = 2\beta_1$), for every value of the pore connectivity, n_T. As the value of θ increases, the values of $v_{pr,i}$ and $v_{prt_o,i}$ are not significantly affected (see Figs. 3 and 4) while the values of $v_{DA,r}$ and $v_{DA,rto}$ are reduced significantly (as the data in Figs. 6 and 7 for D_{pr} and D_{prt_o} would indicate), and thus, the values of the ratios $v_{pr,i}/v_{DA,r}$ and $v_{prt_o,i}/v_{DA,rt_o}$ are increased as θ increases. The values of the ratios $v_{pr,i}/v_{DA,r}$ and $v_{prt_o,i}/v_{DA,rt_o}$ are always enhanced with increasing n_T, in view of the fact that a greater number of alternative pathways is thereby made available to the β-galactosidase molecules being transported in the

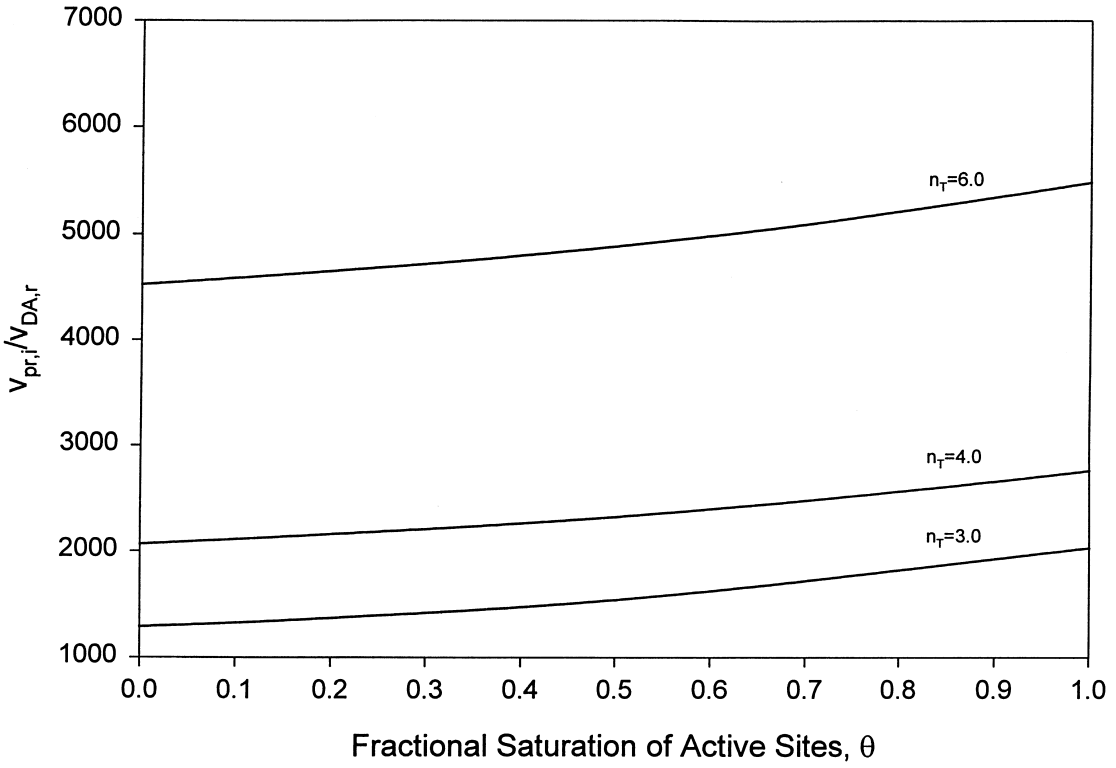

Fig. 9. Ratio of the intraparticle interstitial velocity $v_{pr,i}$ under retained conditions in Adsorbent I ($t_o=0$, $t>0$) to the diffusion velocity $v_{DA,r}$ in the same medium under retained conditions ($t_o=0$, $t>0$) versus the fractional saturation of active sites, θ, and for different values of the pore connectivity, n_T.

intraparticle pores, thus enabling them to bypass narrow pores. The results in Figs. 8–10 clearly indicate that the intraparticle interstitial velocity can substantially enhance the speed of movement of the adsorbate molecules inside the porous structures of Adsorbents I and II, and the enhancement increases as the value of the pore connectivity, n_T, increases.

4. Conclusions and remarks

A cubic lattice network of interconnected pores was constructed to represent the porous structure existing in a monolith (continuous bed) or in a column packed with porous chromatographic particles having intraparticle macropores and micropores. The microscopic properties of the porous network are characterized by the pore size distribution and the pore connectivity, n_T, of the porous medium. Expressions were constructed and utilized to simulate, through the use of the pore network model, the intraparticle interstitial velocity and pore diffusivity of adsorbate molecules in porous chromatographic particles under retained and unretained conditions. The combined effects of steric hindrance at the entrance to the pores and frictional resistance within the pores, as well as the effects of pore size, pore connectivity of the porous network, molecular size of the adsorbate and ligand, and the fractional saturation of adsorption sites (ligands), have been considered. In this work, the adsorbate was taken to be β-galactosidase and two different kinds of adsorption sites were considered. In one case, the adsorbate is adsorbed on the surface of the pores of an ion-exchanger (Adsorbent I). In another case, the β-galactosidase is adsorbed onto anti-β-galactosidase

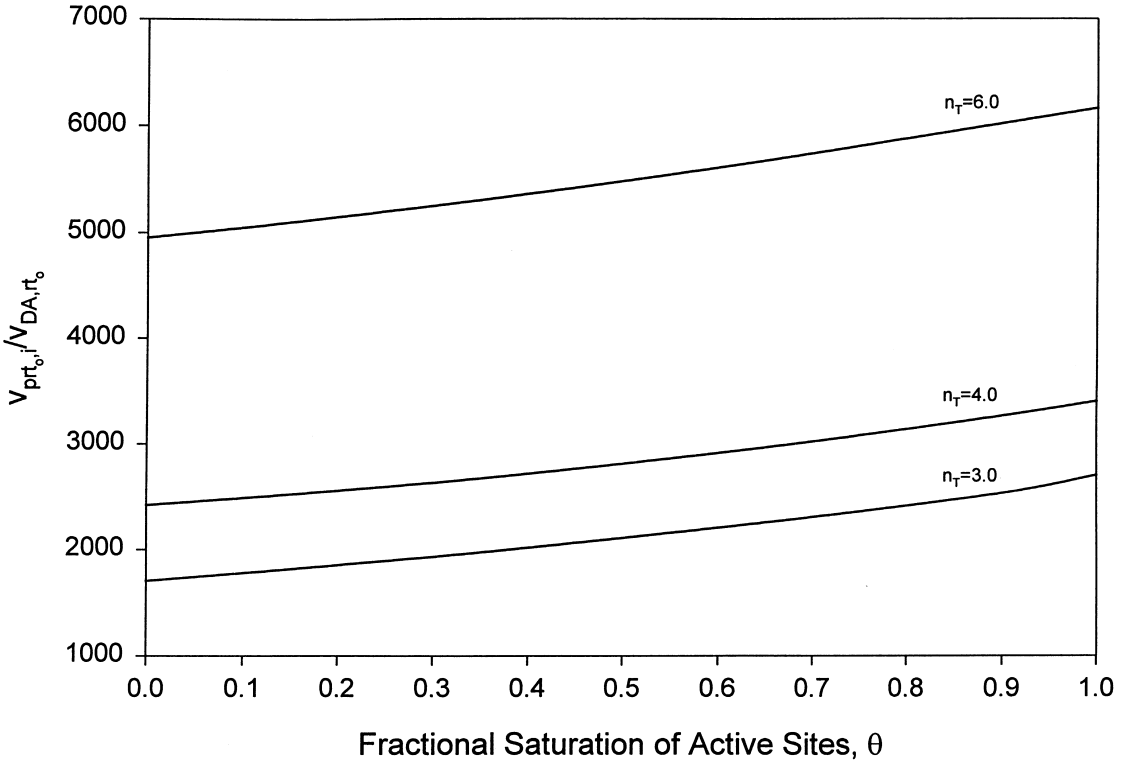

Fig. 10. Ratio of the intraparticle interstitial velocity $v_{prt_o,i}$ under retained conditions in Adsorbent II ($t_o = 2\beta_1$, $t>0$) to the diffusion velocity v_{DA,rt_o} in the same medium under retained conditions ($t_o = 2\beta_1$, $t>0$) versus the fractional saturation of active sites, θ, and for different values of the pore connectivity, n_T.

molecules immobilized on the surface of the pores of the chromatographic particles (Adsorbent II).

The results indicate that for the adsorption systems studied in this work, the obstruction effects on the intraparticle interstitial velocity, due to (i) the thickness, t_o, of the layer of immobilized active sites and (ii) the thickness, t, of the adsorbed layer which is related to the variable θ of the fractional saturation of the active sites, are small and appear to be insignificant when they are compared with the very significant effect that the value of the pore connectivity, n_T, has on the magnitude of the intraparticle interstitial velocity. The effective pore diffusion coefficient of the adsorbate was found to decline with increasing molecular size of ligand, with increasing fractional saturation of the active sites or with diminishing pore size, and with decreasing pore connectivity. The results of this work clearly show that the intraparticle interstitial velocity and the pore diffusivity of the adsorbate increase significantly as the value of the pore connectivity, n_T, increases, and show that the pore connectivity plays a key role in determining the transport of the adsorbate molecules in the porous adsorbent particles under retained and unretained conditions, and therefore, it is an extremely important parameter in the characterization and construction of porous particles. Also, the results of this work show that the magnitude of the intraparticle interstitial fluid velocity is many times larger (orders of magnitude larger) than the diffusion velocity of the adsorbate molecules within the porous particle, and the ratio of the intraparticle interstitial fluid velocity to the diffusion velocity increases significantly as the pore connectivity increases. This result indicates that a certain amount of intraparticle fluid flow would be desirable because it could bring the adsorbate molecules faster to the active sites immobilized on the surface of the pores.

Furthermore, the results indicate that the pore network model and the expressions presented in this work, could allow one to determine the values of the intraparticle interstitial velocity and pore diffusivity of the adsorbate within the porous adsorbent particles, as the fractional saturation of the active sites changes, in an a priori manner, for (a) a given porous adsorbent of interest, (b) a given adsorbate of interest, (c) a given ligand of interest, and (d) a given value of the interstitial column fluid velocity, $V_{b,i}$. This is a very significant result because the numerical values of the intraparticle interstitial velocity and pore diffusivity determined in an a priori manner could be utilized in the macroscopic models [13–20] that could predict the dynamic behavior, scale-up, and design of chromatographic systems employing porous adsorbents. Also, the results obtained from the expressions and pore network modeling approach presented here could have important implications in the selection of a ligand as well as in the selection and construction of an affinity porous matrix, so that the adsorbate of interest can be efficiently separated from a given solution and optimum utilization of the active sites can be achieved.

5. Notation

A adsorbate

B ligand (active site)

C_A concentration of adsorbate A in liquid-filled pores, kg/m^3

$C_{A,i}$, $C_{A,j}$ concentration of adsorbate A at nodes i and j, respectively, kg/m^3

d diameter of bare pore, m

$d_{AB,ij}$ diameter of loaded pore determined from Eq. (18) for the ''t approach'' and from Eq. (19) when $\theta \ll 1$, m

D_A effective pore diffusion coefficient of adsorbate A in a pore, m^2/s

D_{mf} free molecular diffusion coefficient of adsorbate A, m^2/s

D_p effective pore diffusion coefficient of adsorbate A in a porous medium (porous particle) determined from Eq. (34), m^2/s

D_{pr} effective pore diffusion coefficient of adsorbate A in a porous medium (porous particle) under retained conditions ($t>0$) and when $t_o \cong 0$, m^2/s

D_{prt_o} effective pore diffusion coefficient of adsorbate A in a porous medium (porous particle) under retained conditions ($t>0$) and when $t_o>0$, m^2/s

D_{pu} effective pore diffusion coefficient of adsorbate A in a porous medium (porous particle) under unretained conditions ($t=0$) and when $t_o \cong 0$, m^2/s

D_{put_o} effective pore diffusion coefficient of adsorbate A in a porous medium (porous particle) under unretained conditions ($t=0$) and when $t_o>0$, m^2/s

$f(d)$ functional form of pore size distribution (Eq. (1))

$F(C_A)$ equilibrium adsorption isotherm (Eq. (6))

J_{DA} diffusion rate of adsorbate A in a pore, kg/s

$J_{DA,ij}$ diffusion rate of adsorbate A in a pore of length $l_{p,ij}$, kg/s

K_A effective distribution coefficient of adsorbate A with respect to external solution

l_p pore length, m

$l_{p,ij}$ length of pore connecting nodes i and j, m

L lattice size

n_T pore connectivity of the porous network (number of pores connected at a node of the porous network)

N_{DA} mass flux of adsorbate A in a pore due to diffusion, $kg/(m^2 \cdot s)$

$N_{DA,ij}$ mass flux of adsorbate A in a pore of length $l_{p,ij}$ due to diffusion, $kg/(m^2 \cdot s)$

p_i, p_j pressure at nodes i and j, respectively, N/m^2

P permeability of adsorbate A in a porous medium (porous particle), m^2/s

P_{DA} permeability of adsorbate A in a pore, m^2/s

$P_{DA,ij}$ permeability of adsorbate A in a pore of length $l_{p,ij}$, m^2/s

P'_{DA} permeance of adsorbate A in a pore, m^4/s

$P'_{DA,ij}$ permeance of adsorbate A in a pore of length $l_{p,ij}$, m^4/s

Q flow rate through a pore, m^3/s
Q_i flow rate through the interstitial pores in the column, m^3/s
Q_{ij} flow rate through a pore of length $l_{p,ij}$, m^3/s
Q_p intraparticle flow rate, m^3/s
Q_t total flow rate through the bed, m^3/s
r_p radius of bare pore of length l_p, m
$r_{p,ij}$ radius of bare pore of length $l_{p,ij}$, m
R_p radius of porous particle, m
S_c column cross-sectional area, m^2
S_o cross-sectional area of porous medium whose pores are the intraparticle pores, m^2
t thickness of the adsorbed layer, m
t_{ij} thickness of the adsorbed layer in a pore of length $l_{p,ij}$, m
t_o thickness of the layer of active sites (ligands), m
$v_{DA,r}$ diffusion velocity of adsorbate A in the porous medium (porous particle) under retained conditions ($t>0$) and when $t_o \cong 0$, m/s
v_{DA,rt_o} diffusion velocity of adsorbate A in the porous medium (porous particle) under retained conditions ($t>0$) and when $t_o>0$, m/s
$v_{DA,u}$ diffusion velocity of adsorbate A in the porous medium (porous particle) under unretained conditions ($t=0$) and when $t_o \cong 0$, m/s
v_{DA,ut_o} diffusion velocity of adsorbate A in the porous medium (porous particle) under unretained conditions ($t=0$) and when $t_o>0$, m/s
$v_{p,i}$ intraparticle interstitial fluid velocity determined from Eq. (25), m/s
$v_{pr,i}$ intraparticle interstitial fluid velocity under retained conditions ($t>0$) and when $t_o \cong 0$, m/s
$v_{prt_o,i}$ intraparticle interstitial fluid velocity under retained conditions ($t>0$) and when $t_o>0$, m/s
$v_{p,sup}$ superficial intraparticle fluid velocity, m/s
$v_{pu,i}$ intraparticle interstitial fluid velocity under unretained conditions ($t=0$) and when $t_o \cong 0$, m/s
$v_{put_o,i}$ intraparticle interstitial fluid velocity under unretained conditions ($t=0$) and when $t_o>0$, m/s
$\bar{V}_A$ molecular volume of adsorbate A, m^3
V_B molecular volume of ligand B (active site), m^3
$V_{b,i}$ interstitial fluid velocity in column, m/s
$V_{b,sup}$ superficial fluid velocity in column, m/s

Greek symbols

α_1 effective molecular radius of adsorbate A, m
β_1 effective molecular radius of ligand B (active site), m
γ number of ligands (active sites) per unit area of pore wall
ΔC_A concentration difference of adsorbate A between pore ends, kg/m^3
ε void fraction of bed (bed porosity)
ε_p porosity of the porous medium whose pores are the intraparticle pores
ε_t total porosity of the column
θ fractional saturation of ligands (active sites)
μ viscosity of liquid solution, kg/(m·s)
$\varphi(r_p, \alpha_1)$ functional form given in Eq. (4)

Acknowledgements

The authors gratefully acknowledge partial support of this work by Monsanto and the Biochemical Processing Institute of the University of Missouri-Rolla.

References

[1] J.V. Dawkins, L.L. Lloyd, F.P. Warner, J. Chromatogr. 352 (1986) 157.
[2] L.L. Lloyd, F.P. Warner, J. Chromatogr. 512 (1990) 365.
[3] N.B. Afeyan, N.F. Gordon, I. Mazsaroff, L. Varady, S.P. Fulton, Y.B. Yang, F.E. Regnier, J. Chromatogr. 519 (1990) 1.
[4] S.P. Fulton, N.B. Afeyan, N.F. Gordon, F.E. Regnier, J. Chromatogr. 547 (1991) 452.
[5] A.I. Liapis, M.A. McCoy, J. Chromatogr. 599 (1992) 87.

[6] G. Carta, M.E. Gregory, D.J. Kirwan, H.A. Massaldi, Sep. Technol. 2 (1992) 62.
[7] M.A. McCoy, A.I. Liapis, K.K. Unger, J. Chromatogr. 644 (1993) 1.
[8] D.D. Frey, E. Schweinheim, C. Horvath, Biotechnol. Prog. 9 (1993) 273.
[9] G. Carta, A.E. Rodrigues, Chem. Eng. Sci. 48 (1993) 3927.
[10] A.E. Rodriguez, Z.P. Lu, J.M. Loureiro, G. Carta, J. Chromatogr. A 653 (1993) 189.
[11] A.I. Liapis, M.A. McCoy, J. Chromatogr. A 660 (1994) 85.
[12] A.I. Liapis, Math. Modelling Sci. Computing 1 (1993) 397.
[13] A.I. Liapis, Y. Xu, O.K. Crosser, A. Tongta, J. Chromatogr. A 702 (1995) 45.
[14] G.A. Heeter, A.I. Liapis, J. Chromatogr. A 711 (1995) 3.
[15] Y. Xu, A.I. Liapis, J. Chromatogr. A 724 (1996) 13.
[16] G.A. Heeter, A.I. Liapis, J. Chromatogr. A 734 (1996) 105.
[17] G.A. Heeter, A.I. Liapis, J. Chromatogr. A 743 (1996) 3.
[18] G.A. Heeter, A.I. Liapis, J. Chromatogr. A 760 (1997) 55.
[19] G.A. Heeter, A.I. Liapis, J. Chromatogr. A 761 (1997) 35.
[20] G.A. Heeter, A.I. Liapis, J. Chromatogr. A 776 (1997) 3.
[21] P. E. Gustavsson, A. Axelsson, P. O. Larsson, J. Chromatogr. A 795 (1998) 199.
[22] J.J. Meyers, A.I. Liapis, J. Chromatogr. A 827 (1998) 197.
[23] F. Svec, J.M.J. Fréchet, Anal. Chem. 64 (1992) 820.
[24] Q.C. Wang, F. Svec, J.M.J. Fréchet, J. Chromatogr. A 669 (1994) 230.
[25] F. Svec, J.M.J. Fréchet, J. Chromatogr. A 702 (1995) 89.
[26] S.M. Fields, Anal. Chem. 68 (1996) 2709.
[27] H. Minakuchi, K. Nakanishi, N. Soga, N. Ishizuka, N. Tanaka, Anal. Chem. 68 (1996) 3498.
[28] H. Minakuchi, K. Nakanishi, N. Soga, N. Ishizuka, N. Tanaka, J. Chromatogr. A 762 (1997) 135.
[29] P. E. Gustavsson, Ph.D. Dissertation, Department of Pure and Applied Biochemistry, University of Lund, Lund, 1998.
[30] M.P. Hollewand, L.F. Gladden, Chem. Eng. Sci. 47 (1992) 1761.
[31] J.J. Meyers, 1998, Internal Report Number 12, Department of Chemical Engineering, University of Missouri-Rolla, Rolla, MO, USA.
[32] J.J. Meyers, 1998, Internal Report Number 18, Department of Chemical Engineering, University of Missouri-Rolla, Rolla, MO, USA.
[33] J.K. Petrou, J.H. Petropoulos, N.K. Kanellopoulos, A.I. Liapis, in: A.B. Mersmann, S.E. Scholl (Eds.), Proceedings of the 3rd International Conference on Fundamentals of Adsorption, Engineering Foundation, New York, 1990, p. 679.
[34] J.H. Petropoulos, J.K. Petrou, A.I. Liapis, Ind. Eng. Chem. Res. 30 (1991) 1281.
[35] R.P. Mayer, R.A. Stowe, J. Colloid. Sci. 20 (1965) 893.
[36] D.M. Smith, D.L. Stermer, Powder Technol. 53 (1987) 23.
[37] K. C. Loh, D.I.C. Wang, J. Chromatogr. A 718 (1995) 239.
[38] Z. Dagan, S. Weinbaum, R. Pfeffer, J. Fluid Mech. 115 (1982) 505.
[39] J.H. Petropoulos, A.I. Liapis, N.P. Kolliopoulos, J.K. Petrou, N.K. Kanellopoulos, Bioseparation 1 (1990) 69.
[40] E.M. Renkin, J. Gen. Physio. 38 (1954) 225.
[41] K.H. Keller, T.R. Stein, Mathem. Biosci. 1 (1967) 421.
[42] H. Brenner, L.J. Gaydos, J. Colloid Interface Sci. 58 (1977) 312.
[43] E.A. Mason, R.P. Wendt, E.H. Bresler, J. Membr. Sci. 6 (1980) 283.
[44] H.J. Keh, Physico Chemical Hydrodynamics 7 (1986) 281.
[45] W.M. Deen, AIChE J. 33 (1987) 1409.
[46] A.I. Liapis, H. Sadikoglu, O.K. Crosser, J. Chromatogr. A 828 (1998) 345.
[47] W. Norde, Adv. Colloid Interface Sci. 25 (1986) 267.
[48] P.A. Belter, E.L. Cussler, W.S. Hu, Bioseparations — Downstream Processing in Biotechnology, Wiley, New York, 1988.
[49] A.I. Liapis, J. Biotechnol. 11 (1989) 143.
[50] B.J. Horstmann, H.A. Chase, Chem. Eng. Res. Des. 67 (1989) 243.
[51] F.H. Arnold, H.W. Blanch, J. Chromatogr. 355 (1986) 13.
[52] B.H. Arve, A.I. Liapis, AIChE J. 33 (1987) 179.
[53] B.H. Arve, A.I. Liapis, in: A.I. Liapis (Ed.), Fundamentals on Adsorption, Engineering Foundation, New York, 1987, p. 73.
[54] I. Lundström, B. Ivarsson, U. Jonsson, H. Elwing, in: W.J. Feast, H.S. Munro (Eds.), Polymer Surfaces and Interfaces, Wiley, New York, 1987, p. 201.
[55] A.I. Liapis, in: A.B. Mersmann, S.E. Scholl (Eds.), Proceedings of the 3rd International Conference on Fundamentals of Adsorption, Engineering Foundation, 1990, p. 25.
[56] M.A. McCoy, Ph.D. Dissertation, Department of Chemical Engineering, University of Missouri-Rolla, Rolla, MO, 1992.
[57] Y. Xu, Ph.D. Dissertation, Department of Chemical Engineering, University of Missouri-Rolla, Rolla, MO, 1995.
[58] G.A. Heeter, Ph.D. Dissertation, Department of Chemical Engineering, University of Missouri-Rolla, Rolla, MO, 1997.
[59] A.O. Imdakm, M. Sahimi, Chem. Eng. Sci. 46 (1991) 1977.
[60] F.A.L. Dullien, Porous Media: Fluid Transport and Pore Structure, 2nd ed, Academic Press, New York, 1992.
[61] S.D. Rege, H.S. Fogler, Chem. Eng. Sci. 42 (1987) 1553.
[62] N.W. Carlson, J.S. Dranoff, in: A.I. Liapis (Ed.), Proceedings of the 2nd International Conference on Fundamentals of Adsorption, Engineering Foundation, New York, 1987, p. 129.